LIMNOLOGY
and
OCEANOGRAPHY: METHODS

Limnol. Oceanogr.: Methods 2, 2004, 91–101

High-frequency measurement of seawater chemistry: Flow-injection analysis of macronutrients

Burke Hales[1], Alexander van Geen[2], and Taro Takahashi[2]
[1]College of Oceanic and Atmospheric Sciences, Oregon State University, 104 Ocean Administration, Corvallis, OR 97331 USA.
[2]Lamont Doherty Earth Observatory of Columbia University, Rt 9W, Palisades, NY 10964 USA

Abstract

We adapted a commercially available flow-injection autoanalyzer (Lachat Quik-Chem 8000) to measure seawater nitrate concentrations at a rate of nearly 0.1 Hz and phosphate and silicate concentrations at a rate half that. Several minor improvements, including reduced sample-loop size, high sample flushing rate, modified carrier chemistry, and use of peak height rather than peak area as a proxy for nutrient concentration aided in the increase in sampling rate. The most significant improvement, however, was the construction of a copperized cadmium NO_3^- reduction column that had a high surface area to volume ratio and a stable packing geometry. Preliminary results from a cruise in the Ross Sea in austral spring of 1997 are shown. Precision of all three analyses is better than 1%. Comparison of the nutrient concentrations determined by the rapid analysis method described here with traditional discrete analyses shows that nitrate and silicate determined by the two approaches are within a few percent of each other, but that the phosphate concentrations determined by the rapid analysis are as much as 10% lower than those determined by the discrete analyses.

We needed to measure nutrient concentrations in a continuous stream of seawater delivered to a shipboard laboratory from a towed undulating vehicle (the Lamont Pumping SeaSoar [LPS]; Hales and Takahashi 2002) at rates faster than standard flow-injection analysis (FIA) systems could achieve during a field expedition in the Ross Sea, Antarctica. To this end, we modified a Lachat QuikChem 8000 autoanalyzer system to greatly increase its sample throughput. Several minor modifications were important in achieving this goal; the most important of these was the development of a new Cd column for the reduction of nitrate to nitrite.

Oceanographic background—Nitrate, phosphate, and silicate in seawater are the most abundant of the nutrients thought to limit phytoplankton growth in many parts of the oceans. The availability of micronutrients, such as iron, and the presence of grazers in the planktonic community may also be important factors regulating productivity. There are still large areas of the ocean, however, where the supply of these macronutrients is the key factor in determining the timing and magnitude of phytoplankton blooms.

Another important factor shaping the distribution and magnitude of plankton biomass and growth rate is physical forcing on horizontal scales of 10 to 100 km (the mesoscale). Satellite imagery shows significant and coincident variability in surface ocean properties such as temperature and chlorophyll content on these length scales. The development of towed undulating vehicles has led to great advances in high-speed, high-spatial resolution oceanographic survey work (Aiken 1977, 1981, 1985; Dessureault 1975; Hermann and Dauphinee 1980). The most widely used of these systems is the SeaSoar (Pollard 1986; Griffiths and Pollard 1992; Bahr and Fucile 1995; currently marketed by Chelsea Instrument: http://www.chelsea.co.uk), which is capable of undulating between the surface and depths of a few hundred meters while being towed at speeds of 6 to 8 knots. These towed instrument platforms have resulted in significant improvements in the ability of the oceanographic community to measure mesoscale distributions of physical and bio-optical properties of the upper ocean at high speed.

Determining whether the causal link between this mesoscale physical and biological variability is physical concentration of biomass or enhanced supply of nutrients, however, requires measurement of nutrient concentration distributions at similarly

*Phone: (541) 737-8121. Fax: (541) 737-2064. E-mail: bhales@coas.oregonstate.edu

Acknowledgments

Thanks to the Antarctic Support Association and the captain and crew of the *RVIB NB Palmer* for support in the field. Thanks also to W. O. Smith and R. F. Anderson for their direction of the Joint Global Ocean Flux Survey Antarctic Environment and Southern Ocean Process Study program. The analysis of check samples and working standards by L. Gordon and J. Jennings is greatly appreciated. This article's quality has been greatly improved by the thoughtful and thorough comments of four anonymous reviewers. B. Hales was supported in this work by a Department of Energy Global Change postdoctoral fellowship. Ship time was paid by NSF grant OPP-9350684.

high spatial resolution. Until now, most chemical measurements have relied on slow wet-chemical analyses of coarsely spaced discrete samples subsequent to sampling. As a first step to changing this approach, we recently modified a SeaSoar towed undulating vehicle to carry a high-pressure, positive-displacement pump that delivers seawater to a shipboard laboratory via a tube embedded in the towing cable (the Lamont Pumping SeaSoar; Hales and Takahashi 2002), following the pumping sampling system of Friederich and others (Friederich and Codispoti 1987; Codispoti et al. 1991). We demonstrated that the water-column location of samples taken from the seawater stream can be determined to within less than 0.5 m vertically, and that structure with vertical scale of about 1 m can be resolved in the sample stream. Taking advantage of the information present in a sample stream such as that supplied by the LPS requires an increase in the frequency at which nutrient concentrations can be measured: from one measurement every few min (≈ 0.01 Hz), which is typical of standard flow injection or continuous flow analyses, to one measurement every few seconds (≈ 0.1 Hz). This paper describes such an increase in sampling rate and presents preliminary results obtained with the system in the Ross Sea Polynya in November 1997.

Analytical background—The heart of our analytical system was a Lachat QuikChem 8000 FIA autoanalyzer system (http://www.lachatinstruments.com) configured to analyze nitrate, phosphate, and silicate concentrations in discrete samples that we had in our laboratory. Briefly, seawater samples are introduced to the system via a sample loop on an injection valve. The sample flows through the sample loop when the valve is in the load position; when the valve is switched to the inject position, the sample loop is flushed by a distilled water carrier stream that sweeps the sample into the chemistry manifold. There, combination with a suite of reagents results in a colored complex whose concentration is directly proportional to the nutrient of interest. Ultimately, the concentration of the colored complex is determined via its absorbance with an optical detection system and related to the nutrient concentration through calibration with standards of known concentration. The standard approach with this system is to inject large (1 to 2 mL) sample loops, allow full return to the carrier baseline, and numerically integrate between successive baselines to determine peak area. The maximum sampling frequency attainable is < 0.01 Hz (one sample every few minutes).

The Lachat chemical analyses are all essentially FIA modifications of classical wet-chemical colorimetric analyses described in Grasshoff et al. (1983). Nitrate analysis follows a modification of this method by Johnson and Petty (1983); briefly, samples are injected into a carrier stream through an injection valve and then buffered to pH ≥ 8 with an imidazole buffer rather than the ammonium chloride used previously (Grasshoff 1983; Johnson and Petty 1983). Nitrate in the sample is reduced to nitrite in a column packed with copperized cadmium granules. An acidic solution combining sulfanilamide and N-(1-naphthyl) ethylenediamine dihydrochloride is then added to the carrier/sample stream. Nitrite reacts with sulfanilamide to form a variety of diazonium ion complexes, which subsequently react with N-(1-naphthyl) ethylenediamine dihydrochloride to form colored compounds with an absorbance maximum at a wavelength of 520 nm. The absorption at this wavelength is directly proportional to the concentration of nitrate (and any nitrite that may have been originally present) in the seawater sample, up to concentrations of 40 mM.

Phosphate analysis is an FIA implementation of the method of Koroleff (1983*a*). Briefly, phosphate is reacted at pH ≤ 1 with an acidic solution containing ammonium molybdate and potassium antimony tartrate to generate a phospho(antimony:molybdate) complex. This complex is then reduced with a solution of ascorbic acid to form a blue-colored complex that has an absorbance maximum at 880 nm. Absorption at this wavelength is directly proportional to the phosphate in the sample up to concentrations of 2 mM.

Silicate analysis is an FIA implementation of the method described in Koroleff (1983*b*). First a solution of oxalic acid is combined with the sample stream to suppress any interference from phosphate. Then the sample is reacted with an acidic ammonium molybdate at a pH ≈ 3 to form a silicomolybdate complex. This is then reduced with a stannous chloride solution to form a blue-colored complex that has an absorbance maximum at 820 nm. Absorption at this wavelength is directly proportional to the silicate in the sample up to concentrations of 100 mM.

Sampling frequency limitations—Two factors ultimately limit the frequency at which nutrient samples can be analyzed in a FIA system: (1) the ratio of sample volume to carrier flow rate or the sample flow resolution, τ_{ample}, and (2) axial smearing of the sample as it transits through the reaction manifold, τ_{smear}. The effect of these two can be illustrated by envisioning the idealized square-wave pattern that immediately follows discrete injections of a sample into a carrier stream (Fig. 1). Clearly, samples cannot be analyzed more frequently than once every τ_{sample}. For typical FIA flow rates and tube diameters, flow is laminar (Re ≈ 200; turbulent flow begins at Re ≥ 2100). This results in a parabolic velocity distribution of the fluids in the reaction manifold tubing with a maximum at the center of the tube that is twice the mean velocity (Fig. 2A; see also, e.g., Bird et al. 1960), and a zero velocity at the walls. Such a velocity profile pushes the sample at the center of the tube forward faster than that nearer the tube walls, resulting in a smearing of the original square-wave input signal. The longer the sample is subjected to such a velocity distribution, the more smeared it will become, and ultimately the amplitude itself will be decreased (Fig. 2b). The ratio of maximum flow to mean flow requires that the first part of the signal that reaches the detector will get there in about half the time it takes for the mean, which, in turn, means that τ_{smear} will be approximately equal to the total time that a sample resides in the laminar flow environment between injection and detection. In other words, $\tau_{smear} \approx \tau_{flow}$ where τ_{flow}, given by the total

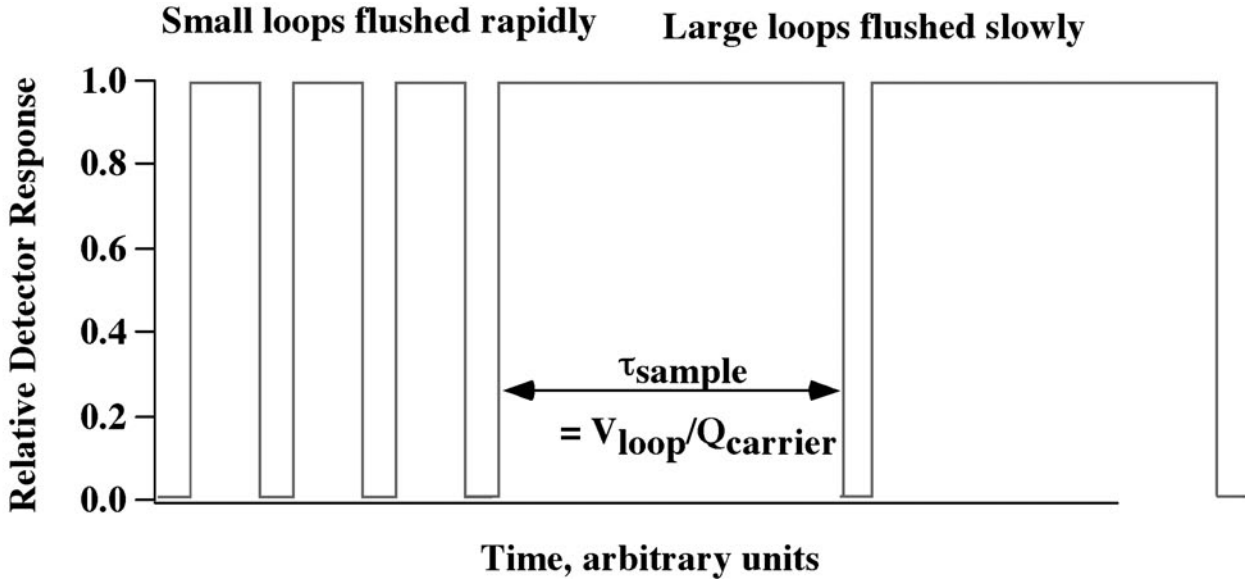

Fig. 1. Schematic representation of the limitation on temporal resolution imposed by τ_{sample}, the time required to flush the sample loop with the carrier solution. If reactions and detector response were instantaneous, a detector immediately downstream from the injection valve would see a square-wave pattern resulting from the alternating load/inject cycle of the valve. Clearly, samples cannot be any closer in time than τ_{sample}, and shorter τ_{sample} leads to higher temporal resolution.

(sample/carrier + reagents) volumetric flow rates divided by the total volume of the reactor system between the injection valve and the detector, is equal to the mean residence time in the system between injection and detection. Other factors that can impact sample smearing are dead volumes and channels in the flow path that can retain or accelerate portions of the sample relative to the average flow.

The above considerations demonstrated the need for small sample sizes, fast flow rates, and short reaction times as the path toward increased sampling frequency. Unfortunately, method sensitivity requirements limit these parameters. Sufficient residence times are required for reactions to progress until a detectable reaction product is reached. Smearing of signals due to these residence times is such that the amplitude of signals from very small sample injections is severely depressed. The key is to limit residence times in reactors to no more than that required for sufficient reaction progress, and then decrease the sample volume to the smallest value that generates sufficient signals for the conditions expected.

Materials and procedures

General modifications—The first modification we made was the replacement of the large (≈1 mL) sample loops on all channels with smaller loops (≈50 mL) made of about 10 cm lengths of 0.030-inch inner diameter (i.d.) × 1/16-inch outer diameter (o.d.) Teflon tubing. The result of this was a substantially reduced injection time required to flush the loop with carrier, and much higher temporal separation between individual injections because of the rapid flushing of the loop with sample during the loading interval. With these small loops and carrier flow rates of a few mL/min, injection periods of only a few seconds are necessary to flush the sample loop several fold with carrier. We tried reducing the sample loop size even more by using smaller i.d. tubing, but this resulted in such a decrease in signal amplitude that we lost sufficient sensitivity, even for the high concentrations we expected to encounter in the Ross Sea.

The second modification was the adaptation of a high-flow rate gear pump to deliver samples at a higher flow rate to all three channels (N, P, and Si) in parallel rather than in sequence. At sample flow rates of about 100 mL/min, the sample loops of all three channels had a flushing time of < 0.1 s. These fast flushing times have two important consequences. First, each sample represents a narrow time window, thus potentially containing very fine resolution information. Second, time synchronization between the three channels is very good—even if the flow doesn't partition itself perfectly equally between the three channels, the maximum temporal offset can only be on the order of the average sample loop-flushing time.

We also modified the distilled water carrier solution in two significant ways. First, we added NaCl until the refractive index of the carrier solution matched that of the seawater sample as closely as possible. This eliminated the erroneous signals leading and following sample peaks due to mixing of carrier and sample with greatly differing refractive indices; these refractive index signals can be large enough to obliterate peaks of very short duration. Second, we buffered the carrier to a pH of about 8, with a combination of $NaHCO_3$ and Na_2CO_3, again roughly matching the seawater condition. This had two benefits. First, matching the seawater pH meant that there were not large pH

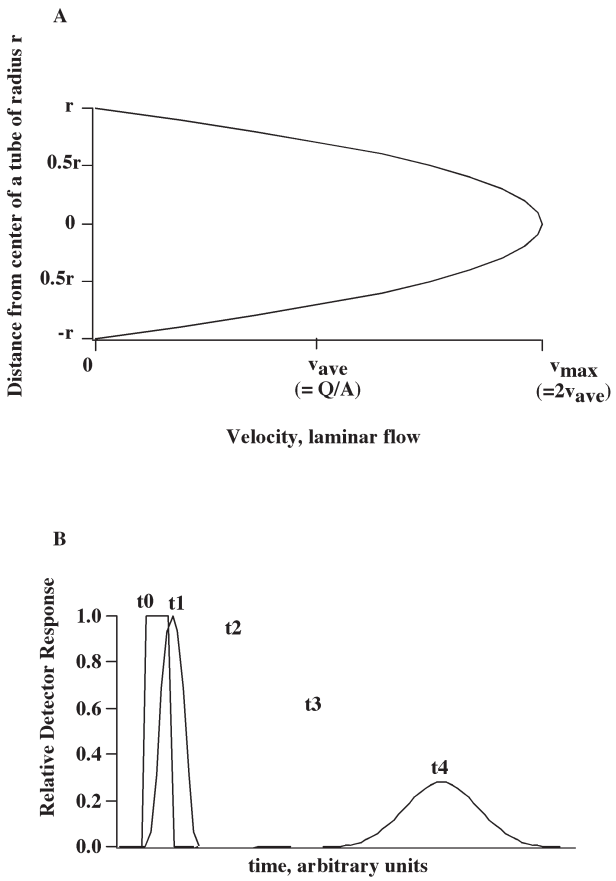

Fig. 2. Schematic representation of the decreased resolution brought about by smearing of the initial square-wave injection signal by laminar flow. Laminar flow in a tube results in a parabolic velocity profile (A) where the velocity at the tube wall is zero, and the maximum velocity, v_{max}, at the tube center is twice the average velocity, v_{ave}, given by the volumetric flow rate Q (mL min^{-1}) divided by the tube cross-section area A (cm^2). The average velocity v_{ave} is the same as the length of the reaction coils divided by the fluid residence time (τ_{flow}, given by V/Q where V is the total volume of the reaction coils). (B) Schematic deterioration of the initial square-wave signal as time in the laminar flow environment increases. For a short time in the system (by t_1), the peak retains the height of the square wave, but the leading and trailing edges are smoothed and broadened. By t_4, the peak is significantly broader and greatly reduced in amplitude. Given the arguments above, the leading edge of the peak will reach the detector about twice as fast as the center of the peak, which will reach the detector approximately τ_{flow} after injection. The temporal width of forward half of the peak will thus be equal to $0.5\tau_{flow}$, and a symmetric peak will have a total temporal width of τ_{flow}.

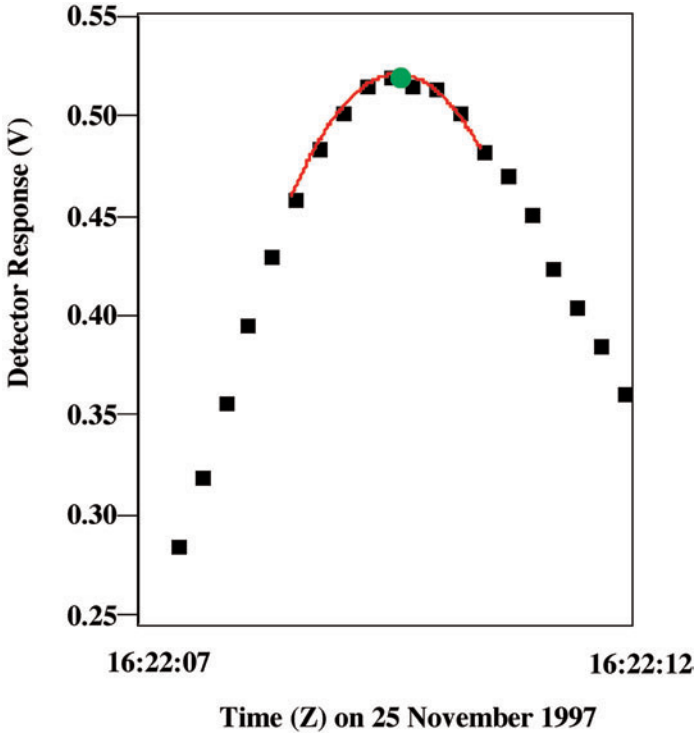

Fig. 3. Illustration of peak height determination. Raw data collected at a rate of 4 Hz (black squares), show the typical peak shape seen at the detector. To reduce the dependence on a single point for defining the maximum peak height, we fit a second-order polynomial curve (red line) to the 9 data points nearest the peak, and calculated the maximum value of that polynomial (green circle).

gradients on leading and trailing edges of the peaks, which could have further decreased reaction extent and overall sensitivity. Second, buffering the carrier pH resulted in greater chemical stability of the copperized Cd reduction column, as the surficial copper is more stable in high-pH solutions.

Finally, we changed the approach to data acquisition and signal processing. One of the greatest limits on temporal resolution is peak integration, which requires full return to baseline between sequential injections. As the trailing edges of FIA peaks often only asymptotically approach the baseline, this can take a long time. Alternatively, using peak height to represent nutrient concentration does not require full return to baseline between injections as long as the previous peak has sufficiently passed so that its "tail" does not add to the maximum value of the current peak. We found maximum peak values by fitting a second-order polynomial through the highest nine measurements in a given peak, and calculating the maximum height from that curve fit (Fig. 3). The "tail" of the preceding peak was found to contribute a few tenths of a percent to the current peak for nitrate, and much less than that for phosphate and silicate.

Nitrate-specific modifications—Rather than pushing each analysis to its highest possible frequency and synchronizing each injection valve for each optimum sampling rate, we chose to focus on improvements to nitrate analysis and to run phosphate and silicate analyses at some integral reduction in frequency relative to nitrate. While phosphate and silicate are each important to primary producers, and in some cases can limit productivity, nitrate is more often thought of as the macro-nutrient limiting productivity over short timescales in the ocean (e.g., Tyrell 1999), and we chose to optimize our

analysis of it as a result. Following the steps outlined below for the nitrate analysis, we were able to run sequential injections of nitrate once every 12 s for a sampling frequency of nearly 0.1 Hz. We then injected the silicate and phosphate sample loops half as often, resulting in a sampling frequency of nearly 0.05 Hz, with each phosphate and silicate injection perfectly correlated with every other nitrate injection.

The first simple modification of the nitrate analysis was to the buffer addition described above. The reduction of seawater nitrate to nitrite in the Cd reduction column is most efficient at pH ≥ 8 (Nydahl 1976). To ensure that the pH remains in this range, an imidazole buffer is added to the carrier/sample stream in the Lachat nitrate manifold immediately downstream of the injection valve. The buffer and carrier/sample stream are then allowed to mix in a long (135 cm; flushing time ≈ 10 s) reaction coil before being introduced to the reduction column. We made two modifications to this approach. First, we eliminated the reaction coil. The kinetics of acid-base reactions are generally transport-limited so there is no need for such a long reaction time. We noticed no significant reduction in column efficiency without the mixing coil, indicating that the solution entering the column was well buffered. Second, we concentrated the buffer solution 4-fold while simultaneously decreasing its delivery rate by a factor of four. This kept the delivery rate of buffer relative to carrier constant, but diluted the sample far less. The volume flow rate of buffer in the standard Lachat manifold was about 75% of the carrier/sample flow rate, which unnecessarily decreases sensitivity, particularly for the short overall reaction times resulting from our attempts to maximize measurement frequency.

The most significant modification to this analysis, however, was reconfiguration of the reduction column. The greatest residence time in the Lachat nitrate chemistry manifold is due to the reduction column, but Johnson and Petty (1983) showed that the reduction of nitrate to nitrite was nearly 100% complete with column residence times of only about 1 s; the large volume of the standard Lachat reduction columns is an obvious volume to minimize. It is straightforward to simply build a smaller column with Cd powder but this has several limitations. First, packing a column with powder is messy and nonquantitative. Second, retention of fine Cd particles in the column during use requires devices such as foam plugs, glass wool, or screens at the column inlet and outlet that are prone to clogging and have complicated flow effects. Third, the granules in the column tend to size-fractionate in response to vibration (such as that experienced on research vessels), which can lead to compaction in, and obstruction of, flow through the column. Finally, column recopperization is difficult if not impossible without disassembling and emptying the Cd powder from the column and then repacking, a challenging chore in the field.

Other researchers have used copperized-Cd tubes in place of the packed column (for example, in the Alpkem RFA systems: http://www.continuous-flow.com). Tubular reductors have the advantages of stable-packing configuration, ease of construction, and on-line re-copperization. However, there are two major shortcomings of these tubular reduction columns: (1) The surface area to volume ratio is low (only 25 cm^2 of surface area for every cm^3 of flow volume in a 1.6-mm (1/16-inch) i.d. Cd tube; the smallest available), requiring long lengths of tube to provide sufficient reduction capacity; and (2) transport of the sample to the walls of the tube is a limiting factor for the reduction reaction—for a 1.6-mm i.d. Cd tube and laminar flow, nearly 3 min is required for a molecule initially at the center of the flow stream to reach the tube wall via diffusion. The residence time necessary for complete reduction of nitrate in a tube would thus be several minutes, even if the reduction kinetics were instantaneous.

We overcame the above shortcomings by packing a bundle of Cd wires in a Teflon tube. Construction was simple. One meter of 0.020-inch (0.5-mm) diameter Cd wire (Alfa-Aesar #11910) was cut into seven equal-length pieces (≈ 14 cm). These were bundled in a hexagonal close-packed geometry, and put inside a 15-cm length of 1/8-inch o.d. × 1/16-inch i.d. Teflon tube. Two short (≤ 0.5 cm) pieces of 0.020-inch (0.5-mm) i.d. × 1/16-inch o.d. Teflon tubing were inserted into each end of the larger tubing and the ends cut flush. This retained the bundle of Cd wires, and decreased the dead-space at the ends of the column. Using a high flow rate pump, we first flushed the column with ethanol, then with distilled water, and finally with 10% HCl to clean the Cd surface. Then we flushed with a solution of 2% $CuSO_4 \cdot 5H_2O$ until the wires appeared uniformly dark gray or black. This only took a few seconds, and care had to be taken that colloidal copper was not formed in the column because it could potentially cause flow blockages. After copperization we flushed the column with pH 10 buffer and capped the ends while still full of buffer for storage.

The resulting column (illustrated in Fig. 4) has a liquid flow volume (tubing volume minus wire volume) of about 0.1 mL compared to the ≈1.5 mL of the Lachat column. It has a surface-area to volume ratio of 100 cm^2/cm^3, which approaches that of packed columns (30 to 1500 cm^2/cm^3 for a column containing coarse [0.3 to 1.5 mm] cadmium granules). The maximum distance between reactive surfaces is about 0.1 mm, similar to that in a packed column, thus reducing the diffusion times required for molecules not initially in contact with the Cd surface to reach said surface within seconds. It is insensitive to vibration, because the wires are continuous and configured in their closest-packed configuration. It is easy to rejuvenate the column without disassembly by simply repeating the flow-through cleaning and copperization procedure described above. It is probably possible to continuously copperize the column while in-line by either adding a short piece of copper tube to the carrier flow path or adding a small amount of copper sulfate to the carrier solution, but we did not try these options.

We verified the column reduction efficiency in two ways. First, we tested for completion of the reduction reaction by examining the sensitivity to residence time in the column. Halving or doubling the column length while leaving the flow

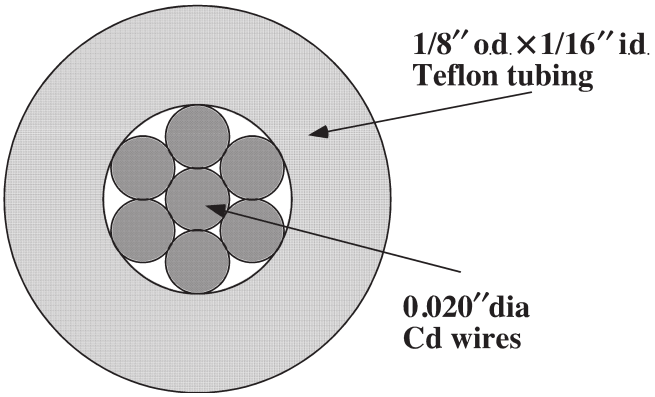

Fig. 4. The Cd reduction column. Seven 0.5-mm (0.020-inch) diameter Cd wires are bundled inside a 1.6-mm (1/16-inch) i.d. Teflon tube, leading to a stable, low dead-volume, high-efficiency reductor.

constant did not significantly change the signal. Therefore the reaction must have been complete for the intermediate column length. Then we tested for column reduction efficiency by running nitrate and nitrite samples of equivalent concentration through the column. The sensitivity to nitrite was indistinguishable from the sensitivity to nitrate, indicating that nearly 100% of the nitrate had been reduced to nitrite in the column.

Assessment and discussion

We took the system to sea in November-December of 1997 as participants in the Joint Global Ocean Flux Survey (JGOFS) Process IV cruise in the Ross Sea Polynya (Smith et al. 2000). Our standardization approach was to run a set of four replicates of each of three different standards for phosphate and silicate and eight replicates each of three different standards for nitrate. Prior to the standards, we flushed the system with the carrier solution and waited long enough for the signals at all the channels to reach a true baseline. Such a sequence, followed by return to sample analysis, is illustrated in Fig. 5. Standardization consisted of subtracting the baseline reading from the standard peak heights and then performing a linear regression of baseline-corrected peak height versus standard concentration. The resulting regression equation was subsequently applied to the baseline-corrected sample peak heights to give nutrient concentration at each measurement time.

We can assess precision of the analyses based on internal measures, e.g., the standard deviation of repeat analyses of standards or of sections of data where we believe the true oceanic concentrations are invariant (such as the deep data in Fig. 6). In either case, we find the precision to be 0.5% to 1% for all three analyses. This, however, is not an independent verification of either the observed relative variability or of the absolute accuracy of the method. One advantage of continuous pumped sampling is the ready availability of water samples that can be analyzed by more standard methods for just such verification. We took several discrete samples over the course of the cruise and had them analyzed by the same continuous-flow auto-analyzer methodology as employed during the JGOFS hydrographic surveys (e.g., Gordon et al. 2000). The results of one such sampling exercise is shown in Fig. 6. To illuminate the agreement between the relative variability seen in the high-frequency data with that seen in the discrete samples analyzed by established methodology, we corrected the discrete sample concentrations to minimize uncertainties in absolute accuracy. This exercise shows that the surface-deep variability, and even much of the smaller-scale variability seen in the high-frequency analyses, is consistent with that quantified by the discrete samples.

Verification of absolute accuracy was more problematic. The correction described above, which was applied uniformly to all discrete measurements of a given type, was only of order 1% for nitrate and silicate analyses, but was nearly 10% for phosphate. Most of the nitrate and silicate discrepancy implied by this correction was accounted for by differences in the apparent standard concentration—i.e., the calculated concentrations of the standards we prepared were about 1% different than the discrete analysis of those standards. Unfortunately, this explained only about half of the discrepancy in phosphate analyses implied by the correction factor applied above. We are left with an unexplained 5% discrepancy between the two measurements, with the rapid-analysis concentrations lower than the discrete samples. We are unsure of the reason for this discrepancy. One possible explanation centers on the fact that the discrete method relied on hydrazine reduction of a phospho-molybdate complex, whereas the rapid analysis method relied on ascorbic acid reduction of a phospho-(antimonyl, molybdate) complex. Although we have not found literature documenting systematic differences between the two, there has apparently been discussion within the nutrient analysis community of such differences with some consensus that the methods including antimony yield concentration estimates are systematically lower than those without (Gordon pers. comm. unref.). Whatever the reason for the discrepancy, we must assume that the problem lies with our new analytical approach and that rigorous quantitative interpretation of this phosphate data may require an adjustment of as much as 0.2 mmol kg^{-1}. We believe, however, that the relative patterns shown by the rapid analysis method will withstand further scrutiny.

The nutrient measurement time was corrected to account for lags associated with seawater sample transit through the LPS tow cable (as shown by Hales and Takahashi 2002) and for the time delay of the individual nutrient analyses. The measurements are then synchronized with the data suite collected with in situ sensors aboard the LPS. Fig. 7 shows a single up/down transect of nitrate, phosphate, and silicate versus depth, corresponding to the calibrated data shown in Fig. 6. All three nutrients show similar vertical structure, with lowest, and nearly constant, concentrations in the mixed layer (40 to 50 m depth, as shown by the profiles of sigma-t) where the chlorophyll concentrations are the highest. Deep-surface decreases in

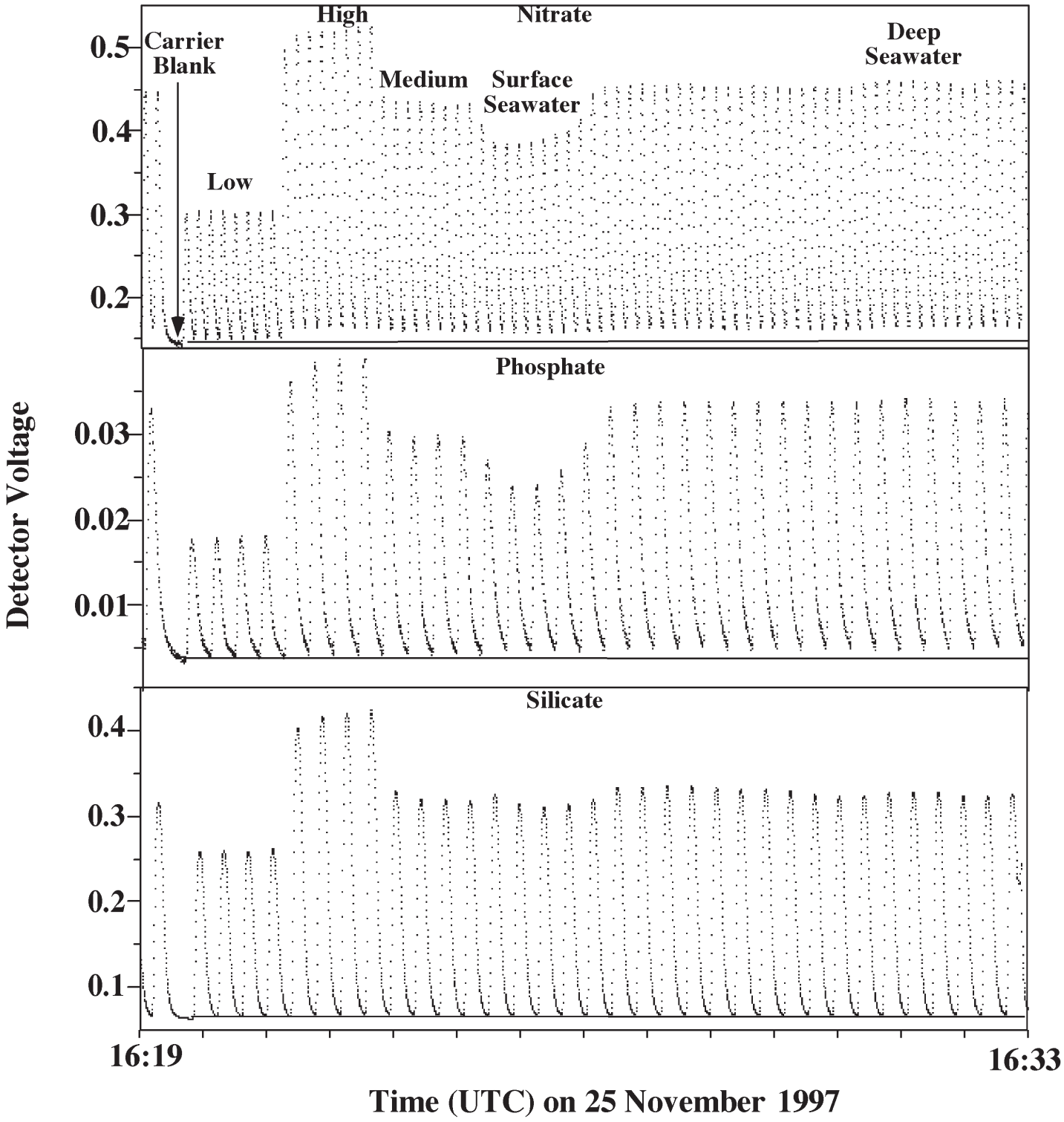

Fig. 5. Raw detector voltage as a function of time for nitrate, phosphate, and silicate. The illustrated sequence shows a few samples, followed by a long flushing of the system with carrier blank to reach baseline (solid horizontal lines in all figures), followed by multiple injections of a low standard, a high standard, and a medium standard, and finally a return to seawater samples. Note that the nitrate system, with sampling frequency of 1/12 s^{-1}, does not quite return to baseline between individual peaks, while the phosphate and silicate systems, with sampling frequency of 1/24 sec^{-1}, very nearly do. Tests of the nitrate system show that the contribution of the "tails" of the leading and following peaks do not contribute significantly to the peak height.

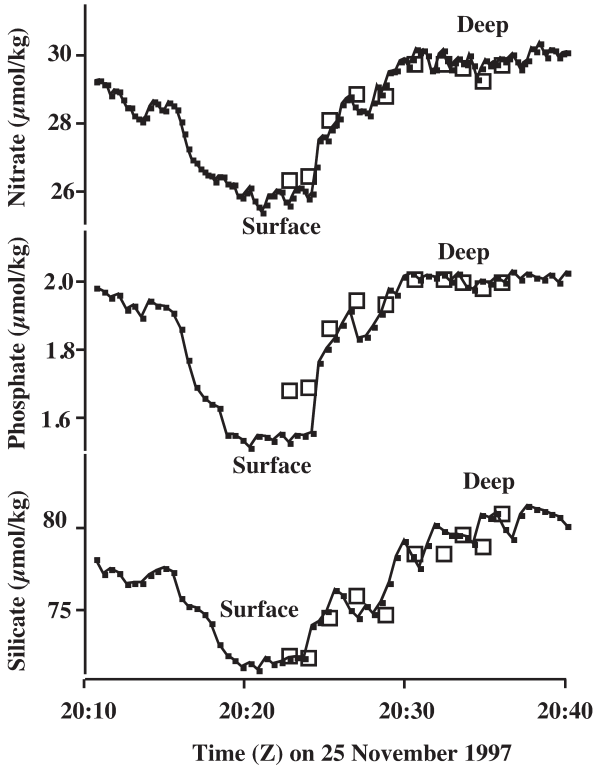

Fig. 6. Example of calibrated nitrate, phosphate, and silicate concentration (small, connected, filled symbols) vs time through an up-down cycle of the LPS, showing depletion of all three nutrients at the surface and enrichment at depth. Discrete check samples (large open symbols) analyzed by L. Gordon and J. Jennings, Oregon State University-COAS, are overlain, demonstrating the quantitative agreement between this method and standard continuous-flow auto-analyzer measurements of discrete samples. Check samples are corrected for lag-time between sample intake at the LPS and the time of check sample collection at the ship-board end of the sample line, and also for temporal offset between the two analyses. Nitrate and silicate check sample concentrations shown had to be corrected downward by about 1% to maximize illustration of agreement with the rapid analyses, and this difference is consistent with the difference between our estimation of standard concentrations and Gordon and Jennings' analyses of these standards. Phosphate check sample concentrations shown, on the other hand, had to be corrected downward by nearly 10%, and this correction exceeds any uncertainty that could be explained by standard inaccuracy.

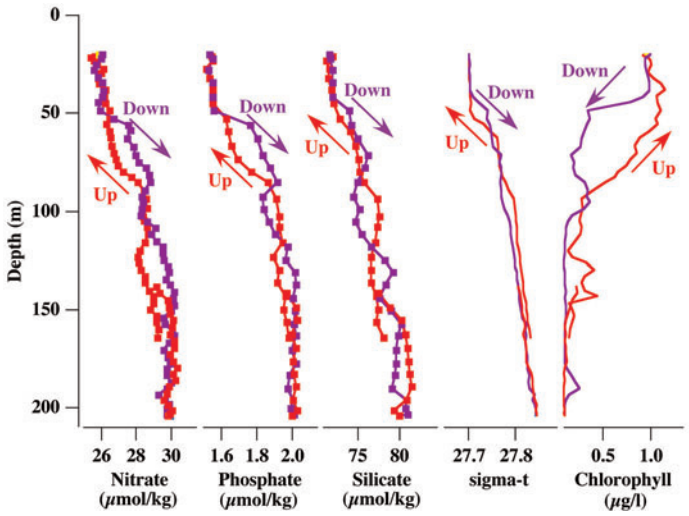

Fig. 7. Vertical profiles of nitrate, phosphate, and silicate, corresponding to the raw data shown in Figure 5 and the calibrated data in Figure 6, along with co-located vertical profiles of in-situ measurements of density anomaly (sigma-t) and chlorophyll concentrations, for a single up-down cycle of the LPS. Measurements made as the LPS ascended are colored red, and those while it ascended colored purple, denoted by similar-colored arrows and text. Note the coherence of the nitrate, phosphate and silicate measurements, and their consistency with the in situ measurements. Nitrate, phosphate, and silicate concentrations are lower and constant in the surface mixed layer where chlorophyll is high, and high at depth where chlorophyll is low. Note also the short length-scale of lateral variability, as evidenced by the difference between vertical distributions of chlorophyll and sigma-t on upward (red) vs downward (purple) samplings of the LPS. The LPS encountered a deeper mixed layer (depth noted by the position of the blue arrows) with higher chlorophyll concentrations and greater nutrient depletion while ascending through the water column, and a shallower mixed layer with lower chlorophyll concentrations and less nutrient depletion while subsequently descending.

nitrate corresponding with productivity in the surface mixed layer are about 10 times the coincident decrease in phosphate, lower than Redfield stoichiometry, but consistent with N:P uptake ratios Southern Ocean diatom-dominated productivity as shown by Bates et al. (1998), Arrigo et al. (1999), Sweeney et al. (2000), and Rubin (2003). The notion that this is diatom-dominated productivity is supported by the deep-surface decrease in silicate concentration, which, at about 8 mmol kg^{-1}, is roughly twice that expected from the canonical 1:1 silicate: nitrate uptake ratio for 'healthy' diatoms (Dugdale and Wilkerson 1998; Takeda 1998), but well within the range of observed ratios for the Southern Ocean (Rubin 2003).

The differences between the up- and down-cast profiles shown in Fig. 7 tantalizingly suggest the importance of short length–scale horizontal variability, even in parameters measured with sensors aboard the LPS. Mixed layer depths (denoted by purple arrows in Fig. 7) are deeper by nearly 10 m on the up-cast (53 m) than on the down-cast (44 m); at 60 m, chlorophyll concentrations are over 0.5 mg L^{-1} higher on the up-cast than on the down-cast. These significant differences occur over very short horizontal scales: at a depth of 60 m, the LPS positions the up-cast and down-cast are separated horizontally by less than a kilometer. The vertical profiles of nutrients are consistent with these physical and bio-optical variations. At 60 m, nitrate and phosphate are lower by about 1.1 and 0.15 mmol kg^{-1}, respectively, on the up-cast than on the down-cast.

Perhaps even more illustrative of the large variability in nutrient concentrations over short length scales is the two-dimensional distribution of nitrate concentration shown in Fig. 8A, sampled during a 20-h LPS survey along 76.5 s in the Ross Sea Polynya on 25 November 1997. The entire region shows striking horizontal variability in the form of "finger"-

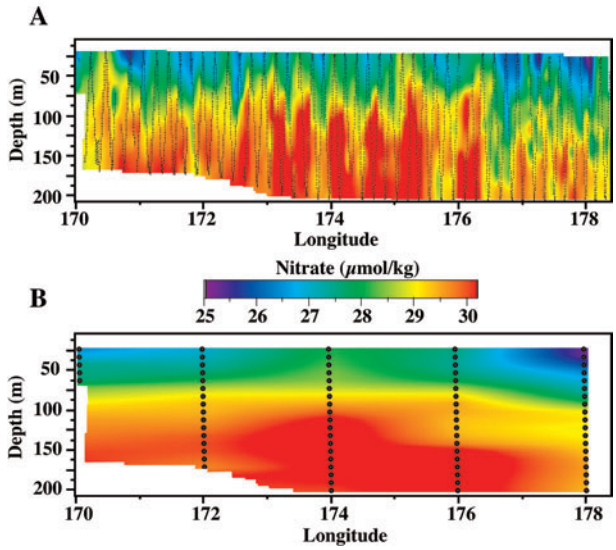

Fig. 8. (A) East-west section of nitrate concentrations along 76.5S in the Ross Sea Polynya on 25 November 1997, as observed using the high-frequency continuous measurement approach described here interfaced with the sample stream provided by the LPS. Small black dots indicate the actual position of samples used in the generation of the gridded section. (B) East-west section of nitrate concentrations along the same transect would be observed by standard hydrographic station sample spacing. This section was constructed by subsampling the section in (A) at the locations indicated by the large black dots in (B), and then filling in the section with a bi-linear interpolation of the subsample.

like plumes of high and low nitrate water, penetrating to depths of 100 m or more, with horizontal scales of several kilometers. A more thorough and quantitative discussion of the mesoscale distributions of physical, biological, and chemical distributions in this region is given by Hales and Takahashi (in press), but a striking qualitative demonstration of the importance of these high spatial-resolution measurements comes from comparing the highly resolved nitrate concentration field shown in Fig. 8a to the field that would result from resampling of the section at 50 km horizontal resolution and 10 m vertical resolution (Fig. 8B). This resolution is comparable to that of the hydrographic sampling of the region during the Ross Sea JGOFS program (Gordon et al. 2000) and corresponds roughly to the resolution that could be attained by such sampling in a one-day time window. None of the variability seen in Fig. 8A is preserved, and most of those features are missed entirely by this section.

Whereas we feel that the rapid FIA approach described here was largely successful, there were numerous problems with this system that should be anticipated and corrected by any user attempting to implement it. These included excessive standard consumption, signal smearing in the high-flow rate sampling pumps, cooling-induced leaking of the injection-valves, sensitivity of the analyses to fluctuations in laboratory temperature, and low overall sensitivity of the analyses to nutrient concentrations. Each of these, and their suggested remedies, are discussed in the following sections.

Comments and recommendations—The first operational problem is that the consumption rate of standards was high. This is because we used the same high-flow rate pump to supply them that we used for the samples. Because the standard concentrations are presumably constant, the fast sampling is probably not necessary and only results in excessive standard use. A simple system involving a solenoid-valve could be used to switch between sample source and standard source, and the standards could be delivered with the reagent/carrier peristaltic pump at a flow rate of only a few mL min^{-1}.

The second is that the pump heads we used for the high-flow sample supply had an appreciable dead volume, which shows up as a slow response to changing standard concentrations. This seems to have been less of a problem for the samples (note the fast return to ambient values following the standard run), probably because the elevated pressure at the sampling port in the LPS line increased flow rates (and hence flushing of the pump head). However, the first replicate of each standard bears some small memory of the preceding sample/standard. This memory is difficult to quantify in the sample-injection approach used here. If we assume that the dynamic response to a step-change in standard concentration can be modeled as a first-order exponential rise (which would be appropriate for the dead-volume flushing scenario discussed above), then we estimate that the response-time for the phosphate and silicate analyses is about 10 s and the response time of the nitrate analyses is about 5 s. Given the proportional difference in injection interval, this means that any one sample may have a memory of the preceding sample, which is equivalent to 10% of the difference between the two. As the continuous analyses rarely experience sequential samples that differ by even as much as 10%, the resulting 1% maximum correction is viewed as insignificant and was not applied. Nonetheless, an identified source of temporal smearing of signals in a system designed specifically to operate at high frequency ought to be eliminated if possible from future applications. We believe that a piston- or plunger-style positive-displacement pump, e.g., as marketed by Fluid Metering Inc. (http://www.fmi-pump.com), as opposed to the gear-style pumps used here, has potential to reduce this problem.

The third is due to a combination of the low temperatures of the Ross Sea and the high flow rates of the sampling pump flushing samples through the sample loop on the injection valve. In concert, these caused a substantial cooling of the Lachat injection valves. The valve heads were made of different material than the valve cores, and their different thermal expansion properties caused them to leak when cooled. We solved this problem by running the samples through a 15-foot coil of 1/16-inch i.d. nylon tube immersed in a beaker of water on a hot-plate. This warmed the samples to approximately room temperature and added only a few seconds of additional lag to the sample time. Whereas this at-sea improvisation worked acceptably in our

application, there was a delicate balance between the hot-plate setting and the sample flow rate. Setting the hot plate too high would excessively heat the samples, causing significant outgassing and bubbling, while setting it too low would insufficiently warm the samples, causing the valves to leak. We suggest that users working in frigid waters should plan to include a thermostated heating system appropriate to the flow rates and temperatures of the high-flow sample line.

Fourth, our Si and N chemistry exhibited some sensitivity to the temperature of the laboratory. Granted, we were doing our work in a particularly poor thermal-controlled setting. Our lab space was in an uninsulated room, heated by a single large blower with wide temperature tolerances, and the only available bench space was situated directly beneath this blower. Further confounding this issue was the fact that this lab was a major walkway from interior labs to the open deck. Frequent opening and intermittent closing of exterior doors led to large temperature swings in the laboratory, which were reflected dramatically in the silicate analysis and to some extent in the nitrate analysis. Phosphate, however, showed no such sensitivity because of the presence of a heated, thermostated block around which the primary reaction coil was wound. One solution is to simply demand better laboratory conditions; however seagoing analytical chemists can't always enforce such demands. The best solution is to add heated, thermostated control to both the N and Si reaction columns.

Finally, the combination of small sample loops and short residence times in reaction volumes led to greatly limited sensitivity. This was not a significant problem in the early-bloom conditions of the Ross Sea where nutrient concentrations were high and also highly variable. Potential users should be cautious, however, about taking such a system to sea in a setting where concentrations and variability are low. Adding the heating elements to the analytical systems, described above, may significantly alleviate this problem as heat speeds chemical reactions and thus reduces the requirement for long reaction times. Other solutions, however, such as increasing sample loop size or increasing reaction residence time, will directly and negatively impact sampling frequency. This remains an unresolved problem with this approach.

References

Aiken, J. 1985. The undulating oceanographic recorder mark 2. A multirole oceanographic sampler for mapping and modeling the biophysical marine environment. Amer. Chem. Soc. 209:315-332.

———. 1981. The undulating oceanographic recorder mark 2. J. Plankton Res. 3:551-560.

———, R. H. Bruce, and J. A. Lindley. 1977. Ecological investigations with the undulating oceanographic recorder: the hydrography and plankton of the waters adjacent to the Orkney and Shetland Islands. Mar. Biol. 39:77-91

Arrigo, K. R., D. H. Robinson, D. L. Worthen, R. B. Dunbar, G. R. DiTullio, M. VanWoert, and M. P. Lizotte. 1999. Phytoplankton community structure and the drawdown of nutrients and CO_2 in the Southern Ocean. Science 283:365-367.

Bahr, F., and P. D. Fucile. 1995. SeaSoar—a flying CTD. Oceanus 38:26-27.

Bates, N. R., D. A. Hansell, C. A. Carlson, and L. I. Gordon. 1998. Distribution of CO_2 species, estimates of net community production, and air-sea CO_2 exchange in the Ross Sea polynya. J. Geophys. Res. 103:2883-2896.

Bird, R. B., W. E. Stewart, and E. N. Lightfoot. 1960. Chapter 2, p. 34-70. *In* Transport phenomena. Wiley.

Codispoti, L. A., G. E. Friederich, J. W. Murray, and C. M. Sakamoto. 1991. Chemical variability in the Black Sea: implications of continuous vertical profiles that penetrated the oxic/anoxic interface. Deep-Sea Res. 38(supp. 2):S691-S710.

Dessureault, J.-G. 1975. Batfish: a depth-controllable towed body for collecting oceanographic data. Ocean Eng. 3:99-111.

Dugdale, R. C., and F. P. Wilkerson. 1998. Silicate regulation of new production in the equatorial Pacific upwelling. Nature 393:270-273.

Friederich, G. E., and L. A. Codispoti. 1987. An analysis of continuous vertical nutrient profiles taken during a cold-anomaly off Peru. Deep-Sea Res. 34:1049-1065.

Gordon, L. I., L. A. Codispoti, J. C. Jennings, F. J. Millero, J. M. Morrison, and C. Sweeney. 2000. Seasonal evolution of hydrographic properties in the Ross Sea, Antarctica 1996-1997. Deep-Sea Res. II 47:3095-3118.

Grasshoff, M. 1983. Determination of nitrate, p. 143-187. *In* K. Grasshoff, M. Erhardt, and K. Kremling, Methods of seawater analysis, Verlag Chemie.

———, K. Erhardt, and K. Kremling. 1983. Determination of nutrients, p. 143-150. *In* K. Grasshoff, M. Erhardt, and K. Kremling, Methods of seawater analysis, Verlag Chemie.

Griffiths, G., and R. T. Pollard. 1992. Tools for upper ocean surveys. Sea Technol. 33:25-32.

Hales, B., and T. Takahashi. 2002. The pumping SeaSoar: a high-resolution seawater sampling platform. J. Oceanic Atmospheric Technol. 19:1096-1104.

——— and ———. In press. High-resolution biogeochemical investigation of the Ross Sea, Antarctica, during AESOPS (U.S. JGOFS) program. Global Biogeochem. Cycles.

Hermann, A. W., and T. M. Dauphinee. 1980. Continuous and rapid profiling of zooplankton with an electronic counter mounted on a 'Batfish' vehicle. Deep-Sea Res. 27:79-96.

Johnson, K. M., and R. L. Petty. 1983. Determination of nitrate and nitrite in seawater by flow injection analysis. Limnol. Oceanogr. 28:1260-1266.

Koroleff, F. 1983*a*. Determination of phosphorus, p. 125-129. *In* K. Grasshoff, M. Erhardt, and K. Kremling, Methods of seawater analysis, Verlag Chemie.

———. 1983*b*. Determination of silicon, p. 174-181. *In* K. Grasshoff, M. Erhardt, and K. Kremling, Methods of seawater analysis, Verlag Chemie.

Nydahl, F. 1976. On the optimum conditions for the reduction of nitrate to nitrite by cadmium. Talanta 23:349-357.

Pollard, R. T. 1986. Frontal surveys with a towed profiling conductivity/temperature/depth measurement package (SeaSoar). Nature 323:433-435.

Rubin, S. I. 2003. Carbon and nutrient cycling in the upper water column across the polar frontal zone along 170° W. Global Biogeochem. Cycles 17:1087-1102.

Smith, W. O., R. F. Anderson, J. K. Moore, L. A. Codispoti, and J. M. Morrison, (2000). The US Southern Ocean Joint Global Ocean Flux Study: an introduction to AESOPS Deep-Sea Res. II 47:3073-3094.

Sweeney, C., W. O. Smith, B. Hales, and others. 2000. Nutrient and carbon removal ratios and fluxes in the Ross Sea, Antarctica. Deep-Sea Res. II 47:3395-3421.

Takeda, S. 1998. Influence of iron availability on nutrient consumption ratio of diatoms in oceanic waters. Nature 393:774-777.

Tyrell, T. 1999. The relative influences of nitrogen and phosphorus on oceanic primary production. Nature 400:525-531.

Submitted 17 June 2003
Revised 5 November 2003
Accepted 12 December 2003